metals

MDPI

Article

FeSiBPNbCu Bulk Nanocrystalline Alloys with High GFA and Excellent Soft-Magnetic Properties

Lei Liu [1,2], Bang Zhou [2], Yiqun Zhang [2,3], Aina He [2,3], Tao Zhang [4], Fushan Li [1,*], Yaqiang Dong [2,3,*] and Xinmin Wang [2]

1 School of Materials Science and Engineering, Zhengzhou University, Zhengzhou 450001, China; liulei123@nimte.ac.cn

2 Zhejiang Province Key Laboratory of Magnetic Materials and Application Technology, CAS Key Laboratory of Magnetic Materials and Devices, Ningbo Institute of Materials Technology & Engineering, Chinese Academy of Sciences, Ningbo 315201, China; zhoubang@nimte.ac.cn (B.Z.); zhangyiqun@nimte.ac.cn (Y.Z.); hean@nimte.ac.cn (A.H.); wangxm@nimte.ac.cn (X.W.)

3 College of Materials Science and Opto-Electronic Technology, University of Chinese Academy of Sciences, Beijing 100049, China

4 Key Laboratory of Aerospace Materials and Performance, School of Materials Science and Engineering, Beihang University, Beijing 100191, China; zhangtao@buaa.edu.cn

* Correspondence: fsli@zzu.edu.cn (F.L.); dongyq@nimte.ac.cn (Y.D.); Tel.: +86-183-3926-8360 (F.L.); +86-574-8761-7212 (Y.D.)

Received: 22 January 2019; Accepted: 8 February 2019; Published: 13 February 2019

Abstract: $(Fe_{0.76}Si_{0.09}B_{0.1}P_{0.05})_{99.3-x}Nb_xCu_{0.7}$ (x = 0–1.5 at. %) bulk nanocrystalline alloys were prepared to investigate the alloying effects of Nb on glass forming ability, thermal stability, soft magnetic properties, and crystallization behavior. It was found that the amorphous forming ability was greatly improved with the addition of minor Nb. The thermal stability of Nb-containing alloy was significantly improved because the initial crystallization temperature and crystallization activation of the primary phase were obviously better than that of the Nb-free alloy. Further, the larger intervals of two-phase crystallization temperature and the significantly higher activation energy of crystallization of the second phase in the Nb-containing alloys favor the formation of a single α-Fe(Si) nanocrystalline structure. Moreover, Nb-containing alloys exhibit excellent soft magnetic properties, including high saturation magnetization of 1.42–1.49 T, low coercivity of around 1.0 A/m, and high permeability of about 18,000 at 1 kHz, which makes the alloys promising soft magnetic materials for industrial applications.

Keywords: bulk nanocrystalline alloys; glass forming ability; high saturation magnetization; magnetic softness

1. Introduction

The energy crisis is the most serious problem in the development of the current world. Therefore, to improve efficiency and reduce power consumption, higher saturation magnetization (B_s) accompanied with excellent soft magnetic properties (SMPs) is strongly required for the magnetic materials used in electrical power supplies and a variety of other industries. Since the $Fe_{73.5}Si_{13.5}B_9Nb_3Cu_1$ (FINEMET) nanocrystalline alloy obtained through crystalization of the corresponding glassy precursors was first reported by Yoshizawa in 1988 [1], Fe-based nanocrystalline alloys have attracted great interest because of their excellent SMPs and extremely low core loss, and thus their low energy consumption and high efficiency [2,3]. Then, a wide variety of new alloys with improved SMPs for electronic and electric industries have been developed through composition adjustment and microstructure evolution, mainly focusing on the FeSiBNbCu, FeSiBCu, and FeSiBPCu

alloy systems [1–7]. Much work has been devoted to studying the mechanism of the nanocrystalline microstructural evolution in these alloys. Hono et al. reported that Cu atoms formed clusters prior to the onset of the crystallization reaction in nanocrystalline FeZrBCu and FeSiBNbCu alloys [8]. By employing a three-dimensional atom probe and a high resolution electron microscope, it was further evidenced that Cu clusters were indirectly making contact with the α-Fe(Si) nanocrystals, suggesting that the α-Fe(Si) particles heterogeneously nucleated at the site of Cu clusters [9]. As Nb was enriched in the remaining amorphous phase, the interface between α-Fe(Si) and the amorphous phase could be clearly seen from the drastic change in the concentrations of Nb, which suppressed the growth of α-Fe(Si) grains.

The mechanical properties of metallic glass, including its intrinsic brittleness, make it difficult to be processed and formed, which seriously limits its practical application in engineering. As recent studies pointed out, the size effects of large ductility and yield strength can be activated for nanoscale thin film metallic glasses and even for micronscale ribbon ones, which exhibit excellent magnetic properties such as much lower magnetic loss than that of their bulk counterpart [10,11]. In fact, it is just thin film metallic glasses and small-scale ribbon ones that are widely used in the power and electronics industries because of their good machinability and formability. However, the glass forming ability (GFA) of these nanocrystalline alloys with high B_s is very low, with the critical diameter (D_{cr}) of fully amorphous rods of no more than 1 mm. This has seriously hindered their further applications, so it is necessary to improve their GFA and SMPs simultaneously. Some attempts have been made to synthesize Fe-based bulk nanocrystalline alloys with high GFA and SMPs. Resultantly, a series of alloys have been successfully developed [12–18], which can be made into thick ribbons or nanocrystalline rod-shaped samples. Recently, by logically adding Cu, FeSiBPNbCu alloys with high GFA and SMPs were successfully developed by our team [18]. Especially when 0.75 at. % Cu was introduced into FeSiBPNb alloy, the alloy after nanocrystalline treatment showed superior SMPs and high GFA. In the combination of Cu and Nb, as widely reported [1,9], Cu offers nucleation sites for the precipitation of the α-Fe(Si) grains, while Nb impedes the growth and promotes these grains to exhibit a much finer scale. Our previous work investigated the influences of Cu element addition point on the GFA of $(Fe_{0.76}Si_{0.09}B_{0.1}P_{0.05})_{99}Nb_1$ and found that the GFA of Cu doped alloys slightly increased with minor Cu addition. Especially for the alloys with Cu content below 1 at. %, the GFA was strong enough to fabricate amorphous rods with diameters of over 1 mm. Further, we tried to increase the content of Fe [19]. The results show that the magnetic saturation of the alloy increased gradually with the increase of iron content, but the GFA of the alloy deteriorated seriously. The increase of 0.02 at. % was no longer sufficient for the preparation of bulk amorphous alloys. Therefore, it is very instructive to study the effect of Nb content on the comprehensive performance in industrial production. In this paper, with the aim of obtaining the high GFA, good SMPs and high B_s alloys, 0.7 at. % Cu was identified as the optimum quantity for the FeSiBPCu system, and the effect of Nb content on the GFA, the SMPs, the thermal stability, and the microstructure of $(Fe_{0.76}Si_{0.09}B_{0.1}P_{0.05})_{99.3-x}Nb_xCu_{0.7}$ (x = 0–1.5) bulk nanocrystalline alloys were systematically studied.

2. Experimental Procedures

$(Fe_{0.76}Si_{0.09}B_{0.1}P_{0.05})_{99.3-x}Nb_xCu_{0.7}$ (x = 0–1.5) alloy ingots were melted by induction melting of pure Fe (99.99 wt. %), Nb (99.9 wt. %) and Cu (99.99 wt. %), crystalline Si (99.99 wt. %) and B (99.9 wt. %) metalloids, and Fe_3P (99.9 wt. %) pre-alloy (Zhongjin, Beijing, China) in a high-purity argon atmosphere. The compositions were nominally expressed in atomic percentage. Cylindrical alloy rods with a constant length of about 40 mm and different diameters ranging between 1 and 3 mm were produced by copper mold casting in an air atmosphere. Amorphous ribbons with a thickness of 22 μm and a width of 1 mm were prepared by the single-roller melt spinning method. The thermal properties of as-cast ribbons were analyzed by differential scanning calorimeter (DSC, 404C, NETZSCH, Selb, Germany) at a heating rate of 0.67 K/s in a high purity argon flow. The annealing temperature (T_a) for the ribbons were determined based on the crystallization temperatures (T_x) obtained from the DSC

test. Isothermal annealing was carried out under certain temperatures for 5 min. On the basis of the DSC curves of as-cast specimens at the heating rates of 0.167, 0.33, 0.5, and 0.67 K/s, the corresponding Kissinger plots of the specimens were used to calculate the activation energy (E_a).

The microstructures of ribbons were examined by X-ray diffraction (XRD, D8 Advance, Bruker, Karlsruhe, Germany) with Cu-Kα radiation and high-resolution transmission electron microscopy (HRTEM, Tecnai G2 F20, FEI, Hillsboro, OR, USA). The samples for TEM observation were prepared by ion milling from both sides of the ribbons. Magnetic properties including B_s, coercivity (H_c), and effective permeability (μ_e) at 1 kHz were measured with a vibrating sample magnetometer (VSM, 7410, Lake Shore, Columbus, OH, USA) under a maximum applied magnetic field of 800 kA/m, DC B-H loop tracer (BHS-40, Riken, Saitama, Japan) under a maximum field of 800 A/m, and an impedance analyzer (4294A, Agilent, PaloAlto, CA, USA) under a field of 1 A/m, respectively. All measurements were performed at room temperature.

3. Results and Discussion

The GFA of $(Fe_{0.76}Si_{0.09}B_{0.1}P_{0.05})_{99.3-x}Nb_xCu_{0.7}$ bulk nanocrystalline alloys was estimated by the D_{cr} of amorphous rods. As shown in Figure 1, the XRD patterns show only a broad peak for Nb-containing alloys, implying the formation of single amorphous structures, but the pattern of Nb-free alloy shows strong crystal characteristics. The D_{cr} fell into the range of 1–2.5 mm with a changing trend that the D_{cr} increased from 1 to 2.5 mm, then reduced to 2 mm depending on the amount of Nb. The GFA was significantly enhanced with minor Nb addition, and the adequate Nb content for the maximum GFA was less than 1 at. % in the alloys. According to the empirical rules of high GFA glass alloys, the addition of Nb caused the more sequential change in the atomic size order, as well as the generation of new atomic pairs with various larger negative heats of mixing between Nb and (Fe, Si, B, P) atomic pairs [20]. Subsequently, a new liquid structure with strong interaction formed and the stronger bonding nature of Nb–(Fe, Si, B, P) atomic pairs was beneficial to suppressing the nucleation and growth reactions of a crystalline phase, leading to the increase in glass transition temperature (T_g) and a supercooled liquid region ($\Delta T_x = T_x - T_g$) [18,19], which can be confirmed by Figure 2. However, the decreases in the GFA could also be attributed to the bonding nature, which becomes too strong when the Nb content is over 1 at. % [20].

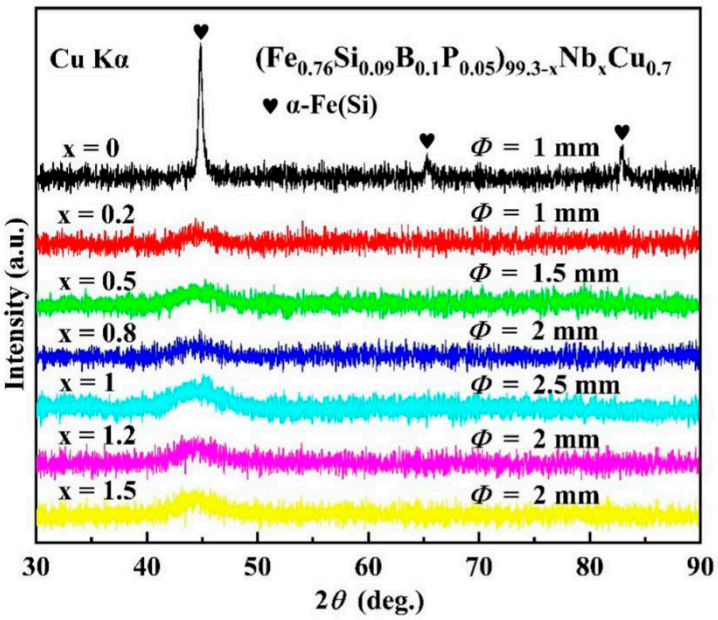

Figure 1. XRD patterns of the as-cast $(Fe_{0.76}Si_{0.09}B_{0.1}P_{0.05})_{99.3-x}Nb_xCu_{0.7}$ (x = 0, 0.2, 0.5, 0.8, 1.0, 1.2, 1.5) rods with different diameters.

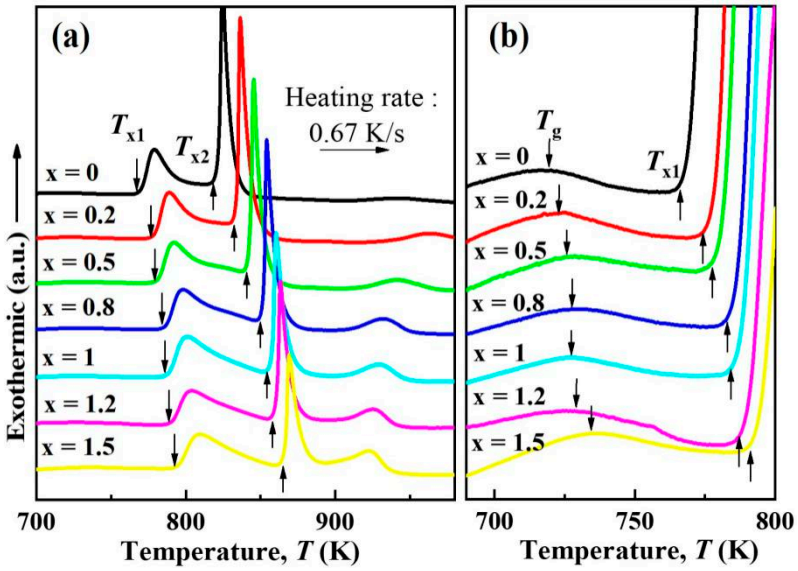

Figure 2. (**a**) DSC curves of the as-cast $(Fe_{0.76}Si_{0.09}B_{0.1}P_{0.05})_{99.3-x}Nb_xCu_{0.7}$ (x = 0, 0.2, 0.5, 0.8, 1.0, 1.2, 1.5) ribbons heated at a rate of 0.67 K/s. (**b**) Enlarged DSC curves showing the supercooled liquid region.

The thermal properties of as-cast ribbons were estimated by DSC at a heating rate of 0.67 K/s, as shown in Figure 2. The pattern of Nb-free alloy exhibits a distinct temperature range between the first and second exothermic peaks and a large area followed by the first crystallization peak, which means that a massive number of α-Fe(Si) crystals were precipitated. This indicates that the $(Fe_{0.76}Si_{0.09}B_{0.1}P_{0.05})_{99.3}Cu_{0.7}$ alloy is an excellent candidate for nanocrystallization. However, the low initial crystallization temperature (T_{x1} = 679 K) and relatively small supercooled liquid region implies low thermal stability against crystallization and thus low GFA. However, the T_{x1} increased by 27 K when the Nb content was up to 1.5 at. %, indicating the significant enhancement of stability. All the samples exhibited observable ΔT_x and followed a trend (initially increasing with the amount of Nb, followed by decreasing), as shown in Figure 2b, with the maximum value of 67 K when the amount of Nb reached 1 at. %. The large ΔT_x favored the high GFA in the Nb-containing alloys. Furthermore, the patterns of all the Nb-containing alloys exhibit obvious intervals between the first two exothermic peak temperatures T_{x2} and T_{x1}, which is defined as ΔT ($\Delta T = T_{x2} - T_{x1}$). The ΔT expanded gradually to about 70 K with the addition of 1.5 at. % Nb.

In order to further investigate the effect of Nb on the thermal stability and crystallization process, the activation energy (E_a) of α-Fe(Si) and Fe–(B, P) phases, represented as E_{a1} and E_{a2}, was derived by kinetic analyses. On the basis of the DSC curves of as-cast ribbons at the heating rates of 0.167, 0.33, 0.5, and 0.67 K/s, the corresponding Kissinger plots of the specimens were constructed through the Kissinger method [21]:

$$\ln\left(T_p{}^2/\beta\right) = E_a/(RT_p) + \ln(E_a/R) - \ln\nu \quad (1)$$

where β, R, E_a, ν, and T_p are the heating rate, gas constant, action energy, frequency factor, and peak temperature of crystallization, respectively. As seen in Figure 3, E_{a1} and E_{a2} were calculated as 280.2 and 413.6 kJ/mol, respectively, for the $(Fe_{0.76}Si_{0.09}B_{0.1}P_{0.05})_{99.3}Cu_{0.7}$ alloy, and 368.9 and 576.3 kJ/mol, respectively, for the $(Fe_{0.76}Si_{0.09}B_{0.1}P_{0.05})_{98.8}Nb_{0.5}Cu_{0.7}$ alloy. The activation energy of the Nb-containing (0.5 at. %) alloy is much higher than that of its counterpart Nb-free sample. Therefore, it is more stable to maintain the amorphous structure of the Nb-containing alloy. Moreover, the ΔE_a ($\Delta E_a = E_{a2} - E_{a1}$) of the Nb-containing alloy (207.4 kJ/mol) is higher than the Nb-free alloy (133.4 kJ/mol) and this is more conducive to maintaining the α-Fe(Si) single-phase structure of the alloy. These improvements are mainly due to the existence of Nb [22]. The weak diffusion ability of Nb atoms and enrichment in the interface between α-Fe(Si) and the amorphous phases greatly

suppress the growth of grains. Furthermore, Nb has a strong affinity with B and P, making the E_a much higher [18,21,22].

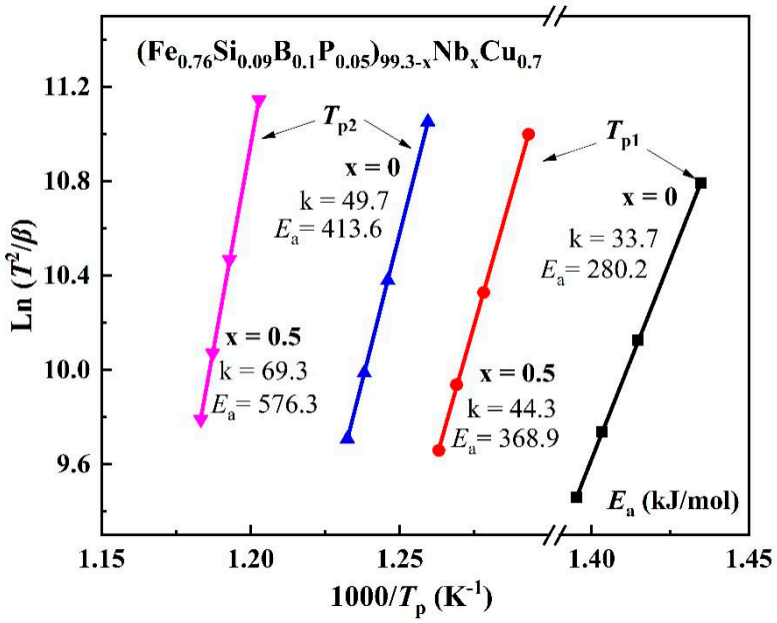

Figure 3. Kissinger plots for the $(Fe_{0.76}Si_{0.09}B_{0.1}P_{0.05})_{99.3-x}Nb_xCu_{0.7}$ (x = 0 and 0.5) ribbons.

The changes in the structure of the Nb-containing amorphous alloy with annealing crystallization were examined by XRD, as shown in Figure 4. The alloy remained in the amorphous state until annealed at 743 K for 5 min. As T_a rose to 763 K, there was only the α-Fe(Si) phase and no other crystallization phases for the alloy could be observed until T_a increased to 803 K. When T_a was elevated to 823 K, the other diffraction peaks emerged, which was in accordance with that of the Fe_3(B,P) phase [18]. The structures of the Nb-containing amorphous alloy after annealing at 783, 803, and 823 K for 5 min were further examined by TEM. After annealing at 783 K for 5 min, as shown in Figure 5a, the crystallization phase is identified as α-Fe(Si) from the the selected area electron diffraction (SAED) patterns in Figure 5d. The α-Fe(Si) grains had an average size of approximately 19 nm, randomly dispersing in the residual amorphous matrix. It can be seen from the TEM image of Figure 5b that the volume fraction of the crystallization phase obviously increased and the residual amorphous matrix relatively decreased when annealed at 803 K, owing to the continuous precipitation and growth of grains. The average size increased to 22 nm and there were not just α-Fe(Si) grains, but a few Fe_3(B,P) grains in the crystallization products, which can be identified from Figure 5d, but failed to be observed by XRD, as shown in Figure 4, as a result of its limited resolution. As T_a increased to 823 K (Figure 5c), the amorphous matrix had almost disappeared, and the α-Fe(Si) and Fe_3(B,P) grains dispersed randomly with an average size of approximately 25 nm. Meanwhile, the heat enthalpy (ΔH) for the two discussed phases decreased continually, meaning the decreasing of the residual amorphous phase, as shown in Figure 5e. The disappearance of the first exothermic peak with T_a indicates that the crystallization of α-Fe(Si) had finished completely, then the second phase began to dominate the crystallization process. In summary, the crystallization evolution of $(Fe_{0.76}Si_{0.09}B_{0.1}P_{0.05})_{98.8}Nb_{0.5}Cu_{0.7}$ ribbon can be summarized as follows:

$$\text{AM} \rightarrow \text{AM}' + \alpha\text{-Fe(Si)}\ (763\ \text{K}) \rightarrow \text{AM}'' + \alpha\text{-Fe(Si)} + Fe_3\text{(B,P)}\ (803\ \text{K}). \quad (2)$$

It can be speculated from the above results that during the annealing process of $(Fe_{0.76}Si_{0.09}B_{0.1}P_{0.05})_{98.8}Nb_{0.5}Cu_{0.7}$, an apparent short-medium range ordering or a nanoscale phase separation came out from the amorphous matrix [23,24], which acted as the nucleation sites

for α-Fe(Si) crystals and led to the refinement of the grains. The introduction of Cu effectively stimulated the precipitation of the α-Fe(Si) nanocrystalline phase, but the addition of Nb significantly inhibited nucleation and growth of grains, then favored the improvement of GFA for the present system [22,25]. Meanwhile, the right amount of Nb addition successfully promoted the acquisition of single and uniform fine α-Fe(Si) grains. Furthermore, Nb played a radical role in this Fe-based bulk nanocrystalline alloys in promoting the formation of α-Fe(Si) nanocrystallites and suppressing compounds such as the (Fe_3(B,P)), hence producing the high-level SMPs of the alloys [26–28].

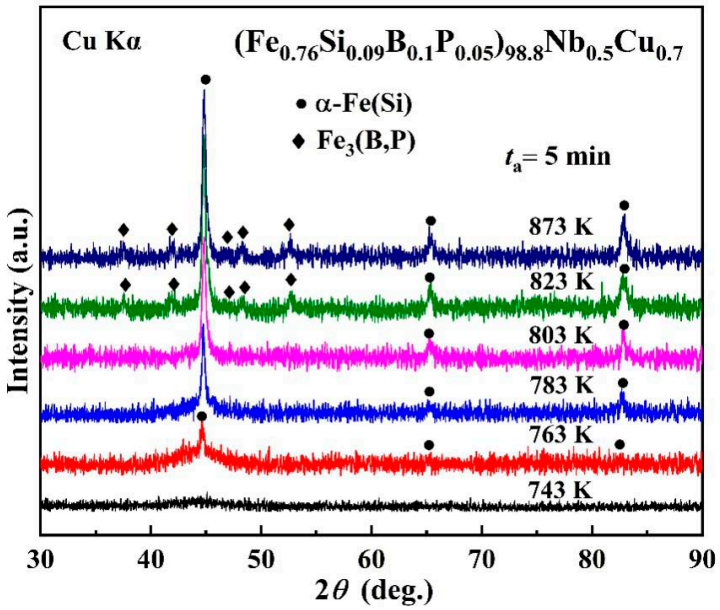

Figure 4. XRD patterns for the $(Fe_{0.76}Si_{0.09}B_{0.1}P_{0.05})_{98.8}Nb_{0.5}Cu_{0.7}$ ribbons after being annealed under several temperatures for 5 min, respectively.

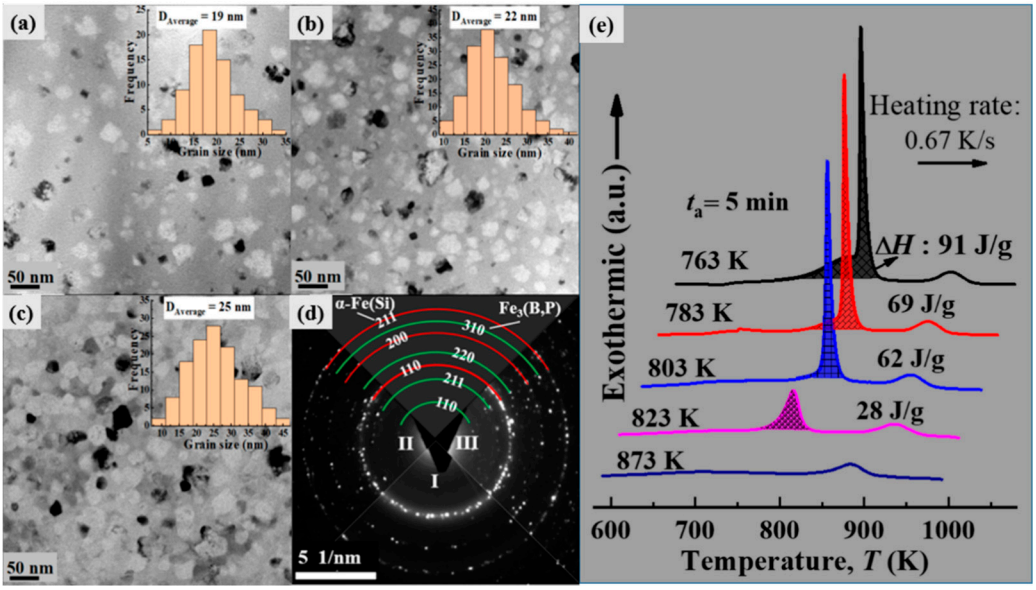

Figure 5. TEM bright field images and grain size distribution for the $(Fe_{0.76}Si_{0.09}B_{0.1}P_{0.05})_{98.8}Nb_{0.5}Cu_{0.7}$ alloy annealed for 5 min under the following: (**a**) 783 K, (**b**) 803 K, and (**c**) 823 K; (**d**) SAED patterns I, II, and III corresponding to 783 K, 803 K, and 823 K, respectively; and (**e**) DSC curves of the annealed ribbons.

Figure 6 illustrates the influences of Nb on B_s and H_c with different T_a for the $(Fe_{0.76}Si_{0.09}B_{0.1}P_{0.05})_{99.3-x}Nb_xCu_{0.7}$ (x = 0–1.5) alloys. Both the B_s and H_c of the Nb-containing alloys showed a trend of decreasing with Nb addition in quenched state or annealed state at different T_a. For both the Nb-containing alloy and the Nb-free one, the B_s changed (Figure 6a) in the trend of increasing first and then decreasing with T_a, while the change of H_c (Figure 6b) showed a contrary trend with the change of B_s. There were no distinct differences in the rate and extent of B_s change between the Nb-containing alloy and the Nb-free one. As the content of Nb increased, B_s increased gradually to the maximum, followed by a slow decrease with T_a going up. Different from the trend of B_s, H_c dropped a lot in the early stage and then slowly decreased to the minimum value and finally increased sharply. Usually, the features of B_s and H_c are considered to be caused by the relaxation of internal stress triggered by low temperature annealing and the appearance of crystallization phases activated by high temperature annealing. When annealed at a low temperature far below T_{x1}, the increase in B_s is mainly attributed to the reduction of free volume and thus the increase of density caused by structure relaxation, while the decrease in H_c is the result of the enhancement of the magnetic isotropy accompanying the internal stress relaxation or removal [29,30]. If annealed at a high temperature over the crystallization peak, the ferroboron phase or ferrophosphorus phase begins to dominate the crystallization process, which is detrimental to SMPs, that is, resulting in the decrease in B_s and the increase in H_c. Thus, the selectable T_a is usually limited within the temperature range of the first crystallization peak, in which the precipitation and growth of fine nano-α-Fe(Si) grains are the objective of optimizing annealing technique. However, the present work indicates that the results of the actual isothermal treatment are quite different from those under the condition of ascending temperature annealing.

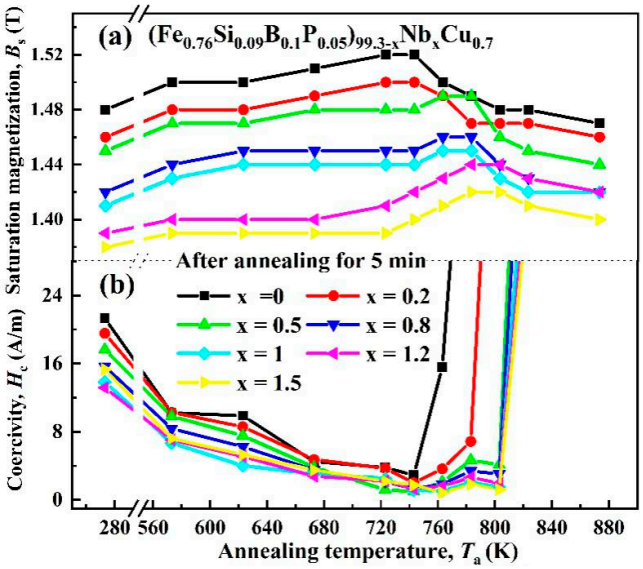

Figure 6. (**a**) B_s and (**b**) H_c of $(Fe_{0.76}Si_{0.09}B_{0.1}P_{0.05})_{99.3-x}Nb_xCu_{0.7}$ (x = 0–1.5) ribbons dependences on T_a annealed for 5 min.

As shown in Figure 2, the crystallization temperature of isothermal annealing was significantly lower (about 20–30 K) than that of ascending temperature annealing, which corresponds to T_{x1} obtained by the corresponding DSC. After annealing in the temperature range of 723–783 K, the Nb-containing alloys showed synthetically excellent SMPs, as shown in Figure 6. Moreover, from Figures 2 and 5, it can be seen that the full removal of stress by annealing in this temperature range resulted in significant improvement of H_c and B_s. The emergence of fine nanocrystals, caused by annealing at higher temperature at this stage, further improved B_s and H_c [31,32]. However, the H_c increased rapidly and the B_s began to decrease upon the emergence of $Fe_3(B,P)$, resulting from annealing at T_a of 783 K or higher.

Table 1 lists the GFA (D_{cr}) and Magnetic Properties (H_c, B_s, and μ_e) of the alloys developed in this work and some other Fe-based bulk nanocrystalline alloys widely reported previously [1,9,13]. The developed FeSiBPNbCu bulk nanocrystalline alloys with minor Nb addition show comprehensively excellent properties, especially for the combination of high GFA and high B_s, namely, D_{cr} of 1–2.5 mm and high B_s of 1.42–1.5 T, but also low H_c of 0.86–2 A/m, high μ_e at 1 kHz of 15,000–18,500. Owing to these advantages, the present alloys are encouraging for future progress as excellent soft magnetic materials.

Table 1. D_{cr} and magnetic properties of the present alloys and some Fe-based bulk metallic alloys reported previously.

Composition (at. %)	D_{cr} (mm)	Magnetic Properties		
		B_s (T)	H_c (A/m)	μ_e
$Fe_{73.5}Si_{13.5}B_9Nb_3Cu_1$ [1]	<1	1.24	0.53	100,000
$Fe_{72.5}Si_{10}B_{12.5}Nb_4Cu_1$ [13]	0.5	1.21	1.8	-
$Fe_{61.5}Co_{10}B_{13.5}Si_{10}Nb_4Cu_1$ [9]	1.5	1.26	5	-
The present alloys:				
$(Fe_{0.76}Si_{0.09}B_{0.1}P_{0.05})_{99.1}Nb_{0.2}Cu_{0.7}$	1	1.5	2	15,600
$(Fe_{0.76}Si_{0.09}B_{0.1}P_{0.05})_{98.8}Nb_{0.5}Cu_{0.7}$	1.5	1.49	0.96	18,500
$(Fe_{0.76}Si_{0.09}B_{0.1}P_{0.05})_{98.5}Nb_{0.8}Cu_{0.7}$	2	1.46	1.28	17,800
$(Fe_{0.76}Si_{0.09}B_{0.1}P_{0.05})_{98.3}Nb_1Cu_{0.7}$	2.5	1.45	1.02	15,500
$(Fe_{0.76}Si_{0.09}B_{0.1}P_{0.05})_{98.1}Nb_{1.2}Cu_{0.7}$	2	1.44	1.3	17,800
$(Fe_{0.76}Si_{0.09}B_{0.1}P_{0.05})_{97.8}Nb_{1.5}Cu_{0.7}$	2	1.42	0.86	16,900

4. Conclusions

FeSiBPNbCu bulk nanocrystalline alloys with high GFA and excellent SMPs were successfully prepared. The feature of crystallization kinetic proved that the addition of Nb significantly improved the thermal stability. It was indicated that the results of the actual isothermal treatment are quite different from those under the condition of ascending temperature annealing. The crystallization temperature of isothermal annealing is significantly lower than that of ascending temperature annealing. The present alloys with minor Nb addition exhibited comprehensively excellent SMPs in both amorphous and nanocrystalline states. Moreover, the alloys developed in this work maintained excellent SMPs over a relatively wide T_a range, which makes them competitive candidates in future applications.

Author Contributions: Conceptualization, F.L. and Y.D.; methodology, L.L. and A.H.; validation, F.L.; formal analysis, L.L. and F.L.; investigation, L.L. and F.L.; resources, Y.D. and X.W.; data curation, L.L. and F.L.; writing—original draft preparation, L.L.; writing—review and editing, F.L. and Y.D.; visualization, B.Z. and Y.Z.; supervision, A.H. and T.Z.; project administration, F.L.; funding acquisition, F.L.

Funding: This work was supported by The National Key Research and Development Program of China (Grant No. 2016YFB0300500); National Natural Science Foundation of China (Grant No. 51601205, 51701183, U1704159, 51571047); and Zhejiang Provincial Natural Science Foundation (Grant No. LQ18E010006).

Conflicts of Interest: The authors declare no conflict of interest.

References

1. Yoshizawa, Y.; Oguma, S.; Yamauchi, K. New Fe-based soft magnetic alloys composed of ultrafine grain structure. *J. Appl. Phys.* **1988**, *64*, 6044–6046. [CrossRef]
2. Gheiratmand, T.; Hosseini, H.R.M. Finemet nanocrystalline soft magnetic alloy: Investigation of glass forming ability, crystallization mechanism, production techniques, magnetic softness and the effect of replacing the main constituents by other elements. *J. Magn. Magn. Mater.* **2016**, *408*, 177–192. [CrossRef]
3. Herzer, G. Modern soft magnets: Amorphous and nanocrystalline materials. *Acta Mater.* **2013**, *61*, 718–734. [CrossRef]

4. Wang, Y.C.; Zhang, Y.; Takeuchi, A.; Makino, A.; Kawazoe, Y. Investigation on the crystallization mechanism difference between FINEMET (R) and NANOMET (R) type Fe-based soft magnetic amorphous alloys. *J. Appl. Phys.* **2016**, *120*, 6. [CrossRef]
5. Ohta, M.; Yoshizawa, Y. Magnetic properties of nanocrystalline $Fe_{82.65}Cu_{1.35}Si_xB_{16-x}$ alloys (x = 0–7). *Appl. Phys. Lett.* **2007**, *91*, 062517. [CrossRef]
6. Makino, A.; Men, H.; Kubota, T.; Yubuta, K.; Inoue, A. New Fe-metalloids based nanocrystalline alloys with high Bs of 1.9T and excellent magnetic softness. *J. Appl. Phys.* **2009**, *105*. [CrossRef]
7. Yu, Q.; Wang, X.D.; Lou, H.B.; Cao, Q.P.; Jiang, J.Z. Atomic packing in Fe-based metallic glasses. *Acta Mater.* **2016**, *102*, 116–124. [CrossRef]
8. Matsuura, M.; Nishijima, M.; Takenaka, K.; Takeuchi, A.; Ofuchi, H.; Makino, A. Evolution of fcc Cu clusters and their structure changes in the soft magnetic $Fe_{85.2}Si_1B_9P_4Cu_{0.8}$ (NANOMET) and FINEMET alloys observed by X-ray absorption fine structure. *J. Appl. Phys.* **2015**, *117*, 4. [CrossRef]
9. Hono, K.; Ping, D.H.; Ohnuma, M.; Onodera, H. Cu clustering and Si partitioning in the early crystallization stage of an $Fe_{73.5}Si_{13.5}B_9Nb_3Cu_1$ amorphous alloy. *Acta Mater.* **1999**, *47*, 997–1006. [CrossRef]
10. Ghidelli, M.; Idrissi, H.; Sébastien, G.; Blandin, J.J.; Raskin, J.P.; Schryvers, D.; Pardoen, T. Homogeneous flow and size dependent mechanical behavior in highly ductile $Zr_{65}Ni_{35}$, metallic glass films. *Acta Mater.* **2017**, *131*, 246–259. [CrossRef]
11. Tian, L.; Cheng, Y.Q.; Shan, Z.W.; Li, J.; Wang, C.C.; Han, X.D.; Sun, J.; Ma, E. Approaching the ideal elastic limit of metallic glasses. *Nat. Commun.* **2012**, *3*, 609. [CrossRef] [PubMed]
12. Aykol, M.; Akdeniz, M.V.; Mekhrabov, A.O. Solidification behavior, glass forming ability and thermal characteristics of soft magnetic Fe–Co–B–Si–Nb–Cu bulk amorphous alloys. *Intermetallics* **2011**, *19*, 1330–1337. [CrossRef]
13. Stoica, M.; Roth, S.; Eckert, J.; Karan, T.; Ram, S.; Vaughan, G.; Yavari, A.R. FeCoBSiNb bulk metallic glasses with Cu additions. *Phys. Status Solidi C* **2010**, *7*, 1331–1335. [CrossRef]
14. Li, J.F.; Shao, Y.; Liu, X.; Yao, K.F. Fe-based bulk amorphous alloys with high glass formation ability and high saturation magnetization. *Sci. Bull.* **2015**, *60*, 396–399. [CrossRef]
15. Inoue, A.; Shen, B.; Ohsuna, T. Soft magnetic properties of nanocystalline Fe-Si-B-Nb-Cu rod alloys obtained by crystallization of cast amorphous phase. *Mater. Trans.* **2002**, *43*, 2337–2341. [CrossRef]
16. Shi, M.; Li, R.; Wang, J.; Liu, Z.; Luo, X.; Zhang, T. Effects of minor Cu addition on glass-forming ability and magnetic properties of FePCBCu alloys with high saturation magnetization. *Philos. Mag.* **2013**, *93*, 2182–2189. [CrossRef]
17. Li, H.X.; Gao, J.E.; Wu, Y.; Jiao, Z.B.; Ma, D.; Stoica, A.D.; Wang, X.L.; Ren, Y.; Miller, M.K.; Lu, Z.P. Enhancing glass-forming ability via frustration of nano-clustering in alloys with a high solvent content. *Sci Rep.* **2013**, *3*, 1983. [CrossRef]
18. Li, Z.; Wang, A.; Chang, C.; Wang, Y.; Dong, B.; Zhou, S. FeSiBPNbCu alloys with high glass-forming ability and good soft magnetic properties. *Intermetallics* **2014**, *54*, 225–231. [CrossRef]
19. Li, Z.; Wang, A.; Chang, C.; Wang, Y.; Dong, B.; Zhou, S. Synthesis of FeSiBPNbCu nanocrystalline soft-magnetic alloys with high saturation magnetization. *J. Alloy. Compd.* **2014**, *611*, 197–201. [CrossRef]
20. Chang, C.; Qin, C.; Makino, A.; Inoue, A. Enhancement of glass-forming ability of FeSiBP bulk glassy alloys with good soft-magnetic properties and high corrosion resistance. *J. Alloy. Compd.* **2012**, *533*, 67–70. [CrossRef]
21. Miao, X.F.; Wang, Y.G.; Guo, M. Structural, thermal and magnetic properties of Fe–Si–B–P–Cu melt-spun ribbons: Application of non-isothermal kinetics and the amorphous random anisotropy model. *J. Alloy. Compd.* **2011**, *509*, 2789–2792. [CrossRef]
22. Ayers, J.; Harris, V.; Sprague, J.; Elam, W.; Jones, H. On the formation of nanocrystals in the soft magnetic alloy $Fe_{73.5}Nb_3Cu_1Si_{13.5}B_9$. *Acta Mater.* **1998**, *46*, 1861–1874. [CrossRef]
23. Nutor, R.K.; Xu, X.J.; Fan, X.Z.; He, X.W.; Lu, X.N.; Fang, Y.Z. Effects of applying tensile stress during annealing on the GMI and induced anisotropy of Fe–Cu–Nb–Si–B alloys. *J. Magn. Magn. Mater.* **2019**, *471*, 544–548. [CrossRef]
24. Ohnuma, M.; Hono, K.; Onodera, H.; Pedersen, J.; Linderoth, S. Cu clustering stage before the crystallization in Fe–Si–B–Nb–Cu amorphous alloys. *Nanostruct. Mater.* **1999**, *12*, 693–696. [CrossRef]

25. Liu, Q.L.; Mo, J.Y.; Liu, H.S.; Xue, L.; Hou, L.; Yang, W.M.; Dou, L.T.; Shen, B.L.; Dou, L.M. Effects of Cu substitution for Nb on magnetic properties of Fe-based bulk metallic glasses. *J. Non-Cryst. Solids.* **2016**, *443*, 108–111. [CrossRef]
26. Hono, K.; Ping, D. Atom probe studies of nanocrystallization of amorphous alloys. *Mater. Charact.* **2000**, *44*, 203–217. [CrossRef]
27. Yang, W.M.; Liu, H.S.; Fan, X.D.; Xue, L.; Dun, C.C.; Shen, B.L. Enhanced glass forming ability of Fe-based amorphous alloys with minor Cu addition. *J. Non-Cryst. Solids.* **2015**, *419*, 65–68. [CrossRef]
28. Hono, K.; Inoue, A.; Sakurai, T. Atom probe analysis of $Fe_{73.5}Si_{13.5}B_9Nb_3Cu_1$ nanocrystalline soft magnetic material. *Appl. Phys. Lett.* **1991**, *58*, 2180–2182. [CrossRef]
29. Inoue, A.; Masumoto, T.; Chen, H. Enthalpy relaxation behaviour of (Fe, Co, Ni) $_{75}Si_{10}B_{15}$ amorphous alloys upon low temperature annealing. *J. Mater. Sci.* **1984**, *19*, 3953–3966. [CrossRef]
30. Ohta, M.; Yoshizawa, Y. High Bs nanocrystalline $Fe_{84-x-y}Cu_xNb_ySi_4B_{12}$ alloys (x = 0.0–1.4, y = 0.0–2.5). *J. Magn. Magn. Mater.* **2009**, *321*, 2220–2224. [CrossRef]
31. Ohta, M.; Yoshizawa, Y. Cu addition effect on soft magnetic properties in Fe–Si–B alloy system. *J. Appl. Phys.* **2008**, *103*, 07E722. [CrossRef]
32. Ohta, M.; Yoshizawa, Y. Improvement of Soft Magnetic Properties in $(Fe_{0.85}B_{0.15})_{100-x}Cu_x$ Melt-Spun Alloys. *Mater. Trans.* **2007**, *48*, 2378–2380. [CrossRef]